# Experimental visualization of scattering at defects in electronic transport through a single atomic junction

Yong-hui Zhang,[1,2,*] Peter Wahl,[1,3] and Klaus Kern[1,4]

[1]*Max-Planck-Institut für Festkörperforschung, Heisenbergstrasse 1, 70569 Stuttgart, Germany*

[2]*Department of Physics, Tsinghua University, Beijing 100084, China*

[3]*SUPA, School of Physics and Astronomy, University of St. Andrews, North Haugh, St. Andrews, Fife KY16 9SS, UK*

[4]*Institut de Physique de la Matière Condensée, Ecole Polytechnique Fédérale de Lausanne (EPFL), CH-1015 Lausanne, Switzerland*

(Received 14 June 2012; published 10 May 2013)

For electronic transport at the nanoscale, coherent scattering at defects plays an important role. Therefore, the capability of visualizing the influence of defects on the conductivity of single atomic junctions may benefit the development of future nano-electronics. Here, we report imaging the coherent scattering from a defect with well-controlled geometry by quantum point contact microscopy recently developed by us. An ∼10% modulation in transport conductance of a single atomic junction is observed, with a phase shift of nearly $\pi$ compared to the tunneling conductance. With the well-defined scattering geometry, we performed a theoretical calculation of the conductance and found the result consistent with the experiment.

DOI: 10.1103/PhysRevB.87.205417 PACS number(s): 72.10.Fk, 73.63.−b, 85.35.−p

## I. INTRODUCTION

As is well known, the rapid growth of the performance and complexity of integrated circuits (IC) is realized by continuous shrinking in the size of the embedded components. Nowadays the dimension of transistors in a CPU has reached a few tens of nanometers. It would therefore be expected that coherent scattering at defects may influence the electronic transport at the nanoscale in future ICs. For mesoscopic systems, coherent scattering leads to universal fluctuations of the conductance as a fundamental characteristic of electronic transport.[1] Scanning probe microscopy has shown that the flow of charge carriers can be interrupted by a tip-induced defect in a semiconductor quantum point contact (QPC) of a submicrometer dimension.[2,3] At the nanoscale, conductance fluctuations in contacts consisting of single atoms or molecules have been observed as a function of applied voltage both using mechanically controlled break junctions (MCBJ)[4] and by scanning tunneling microscopy (STM),[5] which were interpreted in terms of coherent scattering of the charge carriers at defects embedded in the electrodes. However, transport experiments through single atomic junctions with well-controlled scattering geometry of the defects are still missing. This deficiency will be remedied by the quantum point contact microscopy (QPCM)[6] experiment reported in this paper.

## II. EXPERIMENTAL METHODS

Experiments were performed in a low-temperature STM operating at 6.7 K on a polished and oriented Ag(111) single crystal. The Ag(111) surface was prepared by cycles of $Ar^+$ sputtering and annealing to 800 K. Single Ag adatoms were deposited onto the atomically flat Ag(111) surface by controlled tip indentation.[7] QPCM was performed by approaching the STM tip on top of an Ag adatom into contact and then scanning in constant-height mode [see Fig. 1(a) and Ref. 6 for details]. Due to the interaction with the tip apex, the silver atom which forms the point contact stays in the closest hollow site.[8,9] We recorded both the current as well as the differential conductance (through a lock-in amplifier) while scanning the point contact over the surface. The lock-in amplifier was operated at a modulation frequency $f = 9.83$ kHz, an amplitude of $U = 5$ $mV_{rms}$ and a time constant of 10 ms in Figs. 2(d), 2(e), and 3(a) and an amplitude of 20 $mV_{rms}$ and a time constant of 3 ms in Figs. 1(b) to 1(j).

QPCM enables an investigation of transport properties as a function of lateral position with atomic resolution:[6] as is schematically illustrated in Fig. 1(a), a mono-atomic step edge, which can be considered as a one-dimensional defect for the substrate surface, is located at a distance $x$ away from the atomic contact. For a noble metal (111) surface, this leads to the well known standing wave patterns due to quasiparticle interference near the step edge,[10–13] and modulates the conductance $[G(x)]$ of the atomic contact. QPCM can thus measure the conductance modulation with atomic precision in the distance between the defect and the contact.

## III. EXPERIMENTAL RESULTS

Figures 1(b) to 1(e) are differential conductance images of a terrace next to a step edge recorded in tunneling on the Ag(111) sample. They show the well known spatial oscillations of the local density of states (LDOS) due to scattering of quasiparticles at the step edge.[11–14] In the same field of view, the differential conductance of a single atomic junction as a function of distance from the step edge as acquired by QPCM is shown in Figs. 1(f) to 1(i). The QPCM images reveal the atomic structure of the Ag(111) surface superimposed with long-range conductance modulations. The conductance of the atomic contact is close to one conductance quantum ($G_0$) (Refs. 7 and 16); the conductance modulation is about $0.1G_0$ at small distance $x$, and it deceases with distance; the wavelength of the conductance modulation decreases with bias voltage. By comparing conductance traces acquired at the same voltage from QPCM and STM $dI/dV$ images [see Fig. 1(j)], the conductance modulation is found to show a similar wavelength in both cases, however, with a phase shift close to $\pi$. The close relation between QPCM and STM $dI/dV$ images indicates

 

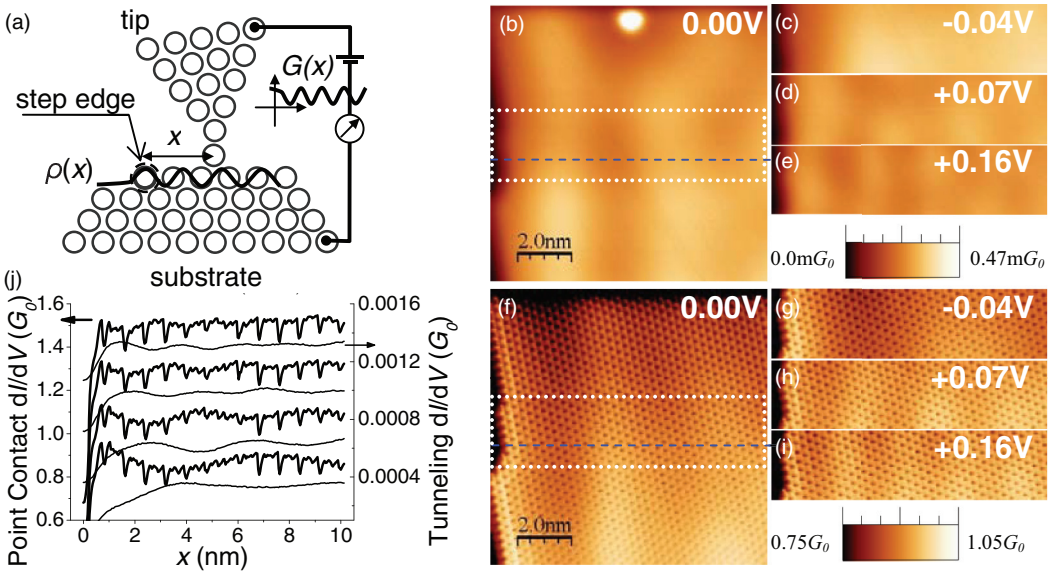


FIG. 1. (Color online) Setup and basic result. (a) Schematic illustration of conductance measurement for a single atomic junction influenced by coherent scattering from a mono-atomic step edge by QPCM. The curve $\rho(\mathbf{r})$ depicts the local density of states of the surface state electrons, resulting in a spatial modulation of the conductance of the atomic point contact, as is depicted by the curve $G(x)$. Circles depict atoms. (b)–(e) Differential conductance ($\mathrm{d}I/\mathrm{d}V$) tunneling images and (f)–(i) $\mathrm{d}I/\mathrm{d}V$ QPCM images acquired in constant height mode in the same area close to a step edge on Ag(111) at different bias voltages. (c)–(e) and (g)–(i) are stripes cut from the original data [see Supplemental Fig. S1 (Ref. 15)] as indicated by the dotted rectangles in (b) and (f). The Ag adatom at the top center of (b) is used for performing QPCM. (j) Conductance line profiles of QPCM images (thick lines) and STM images (thin lines) along a straight line orthogonal to the step edge indicated by dashed lines in (b) and (f). Conductance line profiles taken at different bias voltages (from bottom to top $U = -0.04$, 0.00, 0.07, and 0.16 V), are vertically offset by $0.2G_0$ for QPCM and $3.5 \times 10^{-4}G_0$ for STM. Conductance quantum $G_0 = 2e^2/h = 77.5\ \mu$S.

that the conductance modulation of the atomic contact can be attributed to the oscillatory LDOS resulting from the coherent scattering by the step edge.

For both better characterization and to allow for a detailed comparison between the wavelength and phase of the conductance modulation found in tunneling and contact, we have measured the voltage dependent $\mathrm{d}I/\mathrm{d}V$ in both regimes on the upper terrace along a line perpendicular to the step edge [see Fig. 2(a)]. For the atomic contact this implies laterally manipulating the contact atom to each position where a spectrum is recorded [Figs. 2(b) and 2(c)]. The tunneling spectra are shown in Fig. 2(d) and point contact spectra in Fig. 2(e) as a function of bias voltage and distance from the step edge. The differential conductance at energies below the onset of the surface state relative to the energies above is significantly enhanced in point contact spectra opposite to the behavior in tunneling spectra taken on the clean surface.[17,18]

The interference patterns seen in Figs. 2(d) and 2(e) can be compared to the known dispersion of the surface state. The two-dimensional surface state has a parabolic dispersion with effective mass $m^*$ and onset $E_{\bar{\Gamma}} \equiv E(\mathbf{k} = 0)$. Assuming a perfectly straight step edge, the contribution of the surface state to the LDOS $\rho_s$ including scattering at the step is[11]

$$\rho_s(x, E) = L_0[1 - |r|J_0(2kx)], \tag{1}$$

where $L_0 = \frac{m^*}{\pi\hbar^2}$, $k = \sqrt{\frac{2m^*(E-E_{\bar{\Gamma}})}{\hbar^2}}$, $r = 1$ is the reflection coefficient, $x$ the distance from the step edge, and $J_0$ the Bessel function of the first kind. From Eq. (1) the energy $E_n$ at which the $n$th maximum in the LDOS occurs at distance $x$ is given by

$$E_n(x) = \frac{\hbar^2}{2m^*}\frac{[2\pi(n-1) - \varphi]^2}{4x^2} + E_{\bar{\Gamma}}, \tag{2}$$

where $\varphi$ is an overall phase which equals $-1.25\pi$. The differential conductance measured in tunneling is assumed to be proportional to $\rho_s$. Thus by fitting Eq. (2) to the data in Fig. 2(d), where $m^*$ and $E_{\bar{\Gamma}}$ have been adjusted such that $E_n(x)$ fits the maxima in $\mathrm{d}I/\mathrm{d}V$, we obtain an effective mass of $m^* = 0.37m_e$ and an onset energy of $E_{\bar{\Gamma}} = -0.063$ eV, in good agreement with previous STS studies.[19] To describe the maxima in transport spectra as shown in Fig. 2(e) by Eq. (2), also the phase $\varphi$ has to be adjusted. The same effective mass $m^* = 0.37m_e$ and onset energy $E_{\bar{\Gamma}} = -0.063$ eV are obtained, however, the phase is $\varphi_{\mathrm{PCM}} = (-2.05 \pm 0.1)\pi$, thus the phase shift between point contact and tunneling is $\Delta\varphi_{\mathrm{exp}} = \varphi_{\mathrm{PCM}} - \varphi_{\mathrm{STM}} = (-0.8 \pm 0.1)\pi$. The scattering patterns in the transport and tunneling regime exhibit within the errors the same wavelengths. We do not observe a significant Stark shift, as found for the onset of the surface state in tunneling on the clean surface,[20] even though the measurement in contact is performed at conductances close to one conductance quantum.

The conductance modulation presented in Figs. 1 and 2 has been observed with different atomic structures of the tip apex. For the surface state of Cu(111), similar results can in principle be obtained from combined QPCM and STM measurements. However, the onset energy of the Cu(111) surface state [−0.44 eV (Ref. 11)] is much lower than that of Ag(111). It is difficult for QPCM to measure at large bias voltages as

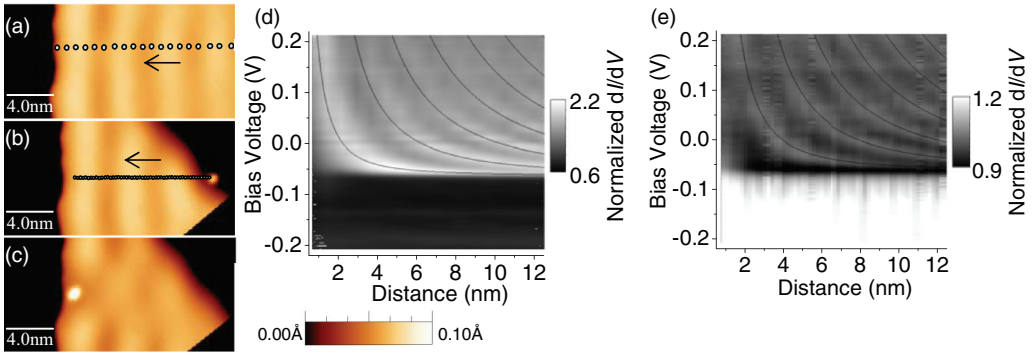


FIG. 2. (Color online) Differential conductance spectra in tunneling and contact as a function of position (a)–(c) STM topographies show the place where tunneling and contact spectra were acquired. ($U = 0.01$ V, $I = 0.11$ nA). Depression in apparent height at the right-top of (b) and (c) is due to the piezo creep. Black at the right-bottom of (b) and (c) is outside the imaging area. (d) Scanning tunneling spectra acquired at the positions approximately indicated by dots in (a), normalized differential conductance is plotted in grayscale (and smoothed) as a function of sample bias voltage and distance from step edge. (e) Point contact spectra acquired at the positions marked in (b), starting from the position of the Ag adatom in the right corner and ending at the step edge in the left. During the measurement, the Ag adatom which forms the contact follows the tip from its position in (b) to that shown in (c). Solid lines in (d) and (e) indicate the positions of local maxima of the standing wave pattern of the Ag(111) surface state according to Eq. (2) [with $m^* = 0.37m_e$, $E_{\bar{\Gamma}} = -0.063$ eV, the position of the step edge $x_0 = -3$ Å, the phase is $\varphi_{\mathrm{STM}} = -1.25\pi$ in (d) and $\varphi_{\mathrm{PCM}} = -2.05\pi$ in (e)].

it will increase the energy dissipation near the atomic contact and thus the tip tends to become unstable. As a result, the Cu(111) surface state has not been investigated to the same level as for Ag(111).

## IV. COMPARISON TO THEORY

Precise knowledge of the scattering geometry enables us to compare the measured conductance fluctuations of a single atomic contact with known theory. The LDOS in STM images is calculated accounting for the interference pattern of the surface state scattered from the step edge.[11] Subsequently, the effect of the quasiparticle interference patterns in the LDOS on the transport through the atomic point contact can be modeled by an Anderson-Newns model considering two adsorbate levels between the tip and the sample representative of the surface atom and the atom at the tip apex.[17,22] Both are assumed to be of the same kind with the adsorbate level at the same energy $\varepsilon_a$. Further, the level of the adatom at the surface is coupled to the surface and bulk bands of the substrate, while the level of the tip atom is coupled to the bulk bands of the tip. Between the two adsorbate levels, a coupling $t$ is assumed. The application of the nonequilibrium Greens function (NEGF) technique yields the transport current as[22]

$$I = \frac{8|e|}{h}|t|^2 \int_{\varepsilon_F}^{\varepsilon_F+eV} d\varepsilon \frac{\mathrm{Im}\Sigma_b \mathrm{Im}[\Sigma_b + \Sigma_s(\varepsilon)]}{|(\varepsilon - \varepsilon_a - eV - \Sigma_b)[\varepsilon - \varepsilon_a - \Sigma_b - \Sigma_s(\varepsilon)] - |t|^2|^2}. \quad (3)$$

The contribution of the bulk states to the self-energy is assumed to be constant ($\Sigma_b = -i\Delta_b$) and to be the same for the tip and surface. The LDOS of the surface state [Eq. (1) with $L_0 = 1$] enters through the self-energy of one of the leads: The imaginary part of the contribution to the self-energy from the surface state is $\mathrm{Im}\Sigma_s = -\Delta_s \rho_s(x,E) * \mathrm{L}(E;\Gamma)$, yielding the real part from a Hilbert transform as $\mathrm{Re}\Sigma_s = \mathsf{H}(\mathrm{Im}\Sigma_s)$, where $\mathsf{H}$ denotes the Hilbert transformation, $\mathrm{L}(E;\Gamma) = \Gamma/[2\pi(E^2 + \Gamma^2/4)]$ is a Lorentzian function, $*$ denotes convolution, and $\Delta_s$ is a constant. The LDOS is convoluted by the Lorentzian $\mathrm{L}(E;\Gamma)$ to account for lifetime broadening, where $\Gamma$ is the inverse lifetime of the surface state. The contribution to the self energy from the surface is $\Sigma_b + \Sigma_s$. Thus the self-energy of the surface includes the scattering at the step edge through the LDOS, but scattering at the contact itself is neglected. For the parameters of the surface state, we use the effective mass $m^*$ and the onset energy $E_{\bar{\Gamma}}$ obtained from our experimental data; $r = 1$[11] and $\Gamma = 7$ meV (Ref. 17). For the parameters of Eq. (3), we use the values given for a silver adatom on Ag(111) in Ref. 17 ($\varepsilon_a = 0.5$ eV, $\Delta_b = 0.8$ eV, and $\Delta_s = 0.5$ eV). The consistency of the calculated conductance modulation with those measured in contact, which is shown below, indicates that neglecting scattering at the point contact is a reasonable assumption.

Figure 3(a) shows the $\mathrm{d}I/\mathrm{d}V$ spectra taken over the center of the silver adatom shown in Fig. 2(b) at different tip-sample separations from tunneling to contact. In comparison, Fig. 3(c) shows the calculated LDOS and transport conductance, which show the same oscillatory behavior, however, with a different phase leading to an almost inverted contrast. Both the experimental and calculated transport spectra show consistently the same basic structure with an enhanced conductance below the onset of the surface state, while above the oscillations due to scattering at the step edge are visible. Notably, the conductance modulation retains the same phase from tunneling to point contact. Thus the phase shift depends on whether the surface

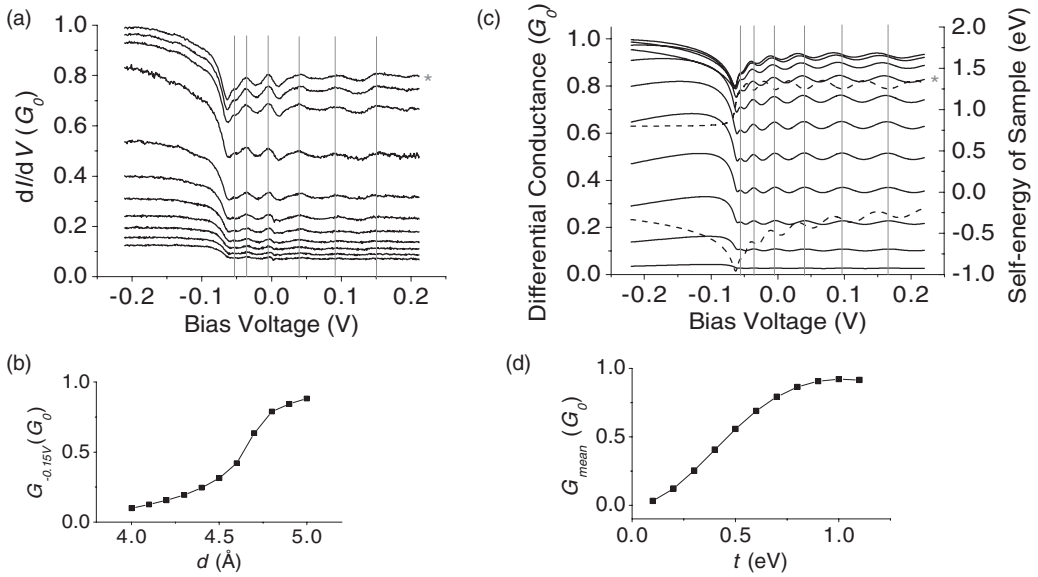


FIG. 3. Conductance modulation as a function of tip-sample distance. (a) Series of $dI/dV$ spectra from tunneling to point contact. The spectra are taken by approaching the tip by different distances over the center of the Ag adatom shown in Fig. 2(b). The wiggles due to coherent scattering of quasiparticles in the surface state are clearly resolved. Vertical lines mark positions of maxima in the conductance trace for comparison. An asterisk to the right marks a spectrum acquired at similar conductance as spectra in Fig. 2(d). Panel (b) shows the conductance at $-0.15$ V of spectra in (a) as a function of vertical tip position $d$, the transition from tunneling to point contact can be clearly identified. Each point in (b) corresponds to a single spectrum in (a). (c) Calculated series of differential conductance spectra according to the model discussed in the text for an adatom at a distance $x = 129$ Å from the step edge [consistent with the distance of the adatom in Fig. 2(b)]. The differential conductance (solid lines) is plotted together with the imaginary part $-\mathrm{Im}[\Sigma_b + \Sigma_s(E)]$ (upper dashed line) and the real part $\mathrm{Re}[\Sigma_b + \Sigma_s(E)]$ (lower dashed line) of the self-energy in Eq. (3). $-\mathrm{Im}[\Sigma_b + \Sigma_s(E)]$ is proportional to the LDOS in Fig. 4(a). Vertical lines mark positions of maxima in the conductance trace for comparison. An asterisk to the right marks a spectrum calculated with the same parameters (in particular $t = 0.8$ eV) as in Figs. 4(a) and 4(c). (d) Mean conductance of spectra in (c) is plotted as a function of tip-adatom coupling $t$. Each point in (d) corresponds to a single spectrum in (c).

state is probed through the contact atom or not,[21] rather than being a specific property of measuring in the transport regime.

Figure 4(a) shows the calculated LDOS and transport conductance at zero bias voltage as a function of distance $x$ from the step edge. Except for $x = 0$, where the atomic contact is lost at the step edge, the long-range conductance modulation from measurements as well as the contrast inversion between QPCM and STM images is nicely reproduced. Figures 4(b) and 4(c) show the calculated LDOS and point contact spectra resembling the ones shown in Figs. 2(d) and 2(e). By fitting Figs. 4(b) and 4(c) the phase shift $\Delta\varphi_{\mathrm{cal}} = \varphi_{\mathrm{QPCM}} - \varphi_{\mathrm{STM}} = (-0.85 \pm 0.1)\pi$ can be obtained, which is consistent with the experimental result $(-0.8 \pm 0.1)\pi$. The consistency between the experiment and theory confirms that the conductance modulation measured by QPCM is well described by the theory.

The phase shift of nearly $\pi$ between the LDOS and transport conductance is rather counterintuitive. To gain some physical insight, the differential conductance of the single atomic junction is explored by calculating its dependence on model

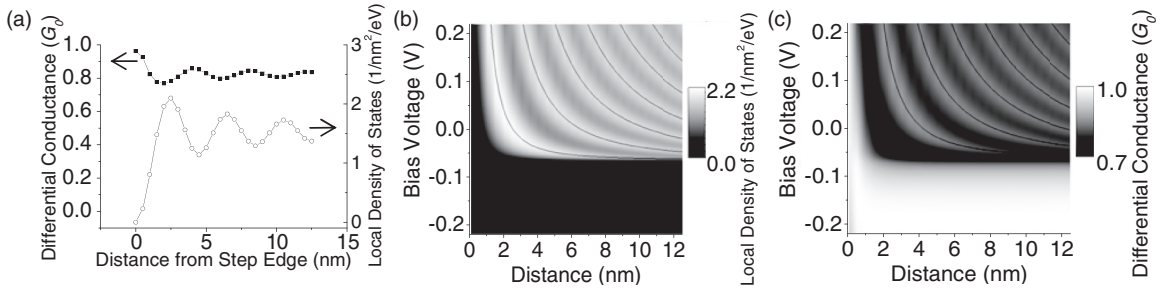


FIG. 4. Theoretical calculation for the scattering pattern in Fig. 2. (a) Model traces for the differential conductance at zero bias voltage in tunneling (empty circle) and in point contact (solid square). The phase shift between the traces in tunneling and point contact is clearly seen. The step edge is assumed to be a black dot scatterer (Ref. 11). (b,c) Bias dependence of the scattering pattern in tunneling [LDOS according to Eq. (1)] and point contact [according to Eq. (3)] plotted in the same way as in Figs. 2(d) and 2(e), respectively. Local maxima are plotted according to Eq. (2) [with $m^* = 0.37m_e$, $E_{\bar{\Gamma}} = -0.063$ eV, the phase is $\varphi_{\mathrm{STM}} = -1.25\pi$ in (b) and $\varphi_{\mathrm{PCM}} = -2.1\pi$ in (c)].

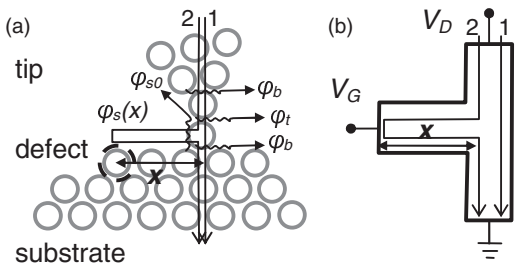


FIG. 5. Model for phase shift and QUIT. (a) Interpretation of the phase shift due to interference of two distinct paths 1 and 2 between tip and substrate. Circles depict atoms; curly lines depict phase shifts from bulk states to adsorbate $\varphi_b$, between adsorbates $\varphi_t$, from surface state to adsorbate $\varphi_{s0}$, and inside surface state $\varphi_s(x)$. (b) Schematic of QUIT following Refs. 25–27.

parameters ($\varepsilon_a$, $\Delta_b$, $\Delta_s$, and $t$) in Eq. (3). The calculation results (see Supplemental Figs. S2 to S4) are summarized in the Supplemental Tables S1 to S4.[15] The calculated phase shift $\Delta\varphi_{\text{cal}}$ is found to depend mainly on the energy of the adsorbate level ($\varepsilon_a$) and—through the width of the adsorbate level—on the coupling to the bulk states ($\Delta_b$). It appears that, for resonant transport (e.g., $|\varepsilon_a| \ll \Delta_b$), $\Delta\varphi_{\text{cal}}$ is close to $\pi$, while it is rather close to 0 for off-resonant transport (e.g., $|\varepsilon_a| \gg \Delta_b$). Therefore the calculation suggests that the phase shift close to $\pi$ is a property of resonant transport through the single atomic junction. On the other hand, off-resonant transport is expected to be relevant, e.g., for rare gas atoms[23] or molecules which do not have a state at the Fermi level.[24]

## V. PRACTICAL IMPLICATION OF THE RESULTS

Our measurement can be interpreted as an interferometric determination of the phase shift associated with the transmission from the adsorbate level to the surface state. In the model depicted by Fig. 5(a), the interference of two different paths [labeled 1 and 2 in Fig. 5(a)] between the tip and the substrate yields the total transmission. Path 2 includes going in and out of the surface state and path 1 does not, thus the phase difference between the two paths is $\varphi_{\text{PCM}} = 2\varphi_{s0} + \varphi_s(x)$, where the $\varphi_{s0}$ and $\varphi_s(x)$ are described in Fig. 5(a). With similar considerations tunneling to the clean surface lead to a phase difference of $\varphi_{\text{STM}} = \varphi_s(x)$. Thus the measured phase difference between these two measurement geometries is $2\varphi_{s0}$ and accounts for the phase shift due to transmission through the adsorbate level to the surface state. The determination of the phase shift is possible because the quantum interference patterns can be compared between the measurements in tunneling and in contact, providing a direct link between the scattering geometry and its influence on quantum transport through a single atom junction.

Furthermore, the measurement setup depicted in Fig. 5(a) bears striking similarities to the proposal [Fig. 5(b)] of a quantum interference transistor (QUIT),[25–27] where changes in the quantum interference occurring in a side arm to the main transport channel—in our case the surface state constitutes the side arm—are used to switch the conductance between the source and drain—in our case the tip and substrate. In the case of QUIT, the length of the side arm is controlled by a gate voltage, whereas here it can be controlled by the position of the adsorbate. It could be envisioned that in realizations with a gated two-dimensional electron gas (2DEG), the conductance could also be tuned by changing the Fermi wave vector. While in the geometry studied here changes in the conductance are only on the order of 10%, this effect is expected to be dramatically increased, e.g., in resonator structures assembled by atomic manipulation, where the modulation of the LDOS becomes stronger.[14,21] Compared to QUIT devices studied previously (see, e.g., Ref. 28), by using a point contact in the geometry discussed here a reduction in size to the ultimate atomic scale becomes conceivable.

In the semiconductor industry, noble metals are widely used in the fabrication of ICs: Since 1997[29] copper interconnects have been used to transport charges between various electronic devices embedded in very large-scale integrated circuits, based on which CPUs in most recent desktop/laptop computers are built. Noble metals are also used as materials for electrodes and gates in the research of nanoelectronic devices. In this work, both the experiment and calculation were performed solely for noble metal surface states [Ag(111) in particular] scattered from a one-dimensional (1D) defect, but they are versatile and are in principle applicable to study the charge transport through single atomic junctions of other materials, or with complicated scattering geometry in the electrode.

As more and more transistors are integrated into the same area of a silicon die, embedded electrical devices and interconnects are becoming smaller. One would expect they eventually shrink down to the size of a few nanometers or even a few angstroms. Consequently, the knowledge of how atomic defects change the conductance of both an electrical device and interconnect may become important for the design of future ICs. In this regard, both the conductance modulation we observe and the QPCM method may find their application in the design of future ICs and nanoelectronic devices, where defects play an important role in the electronic transport at the atomic scale.

## ACKNOWLEDGMENTS

P.W. acknowledges discussions with W. Belzig. Y.Z. acknowledges support by the Chinese Scholarship Council.

*Correspondence should be addressed to: zhangyonghui02@tsinghua.org.cn

[1] Y. Imry, *Introduction to Mesoscopic Physics* (Oxford University Press, New York, 1997).

[2] M. A. Topinka, B. J. LeRoy, S. E. J. Shaw, E. J. Heller, R. M. Westervelt, K. D. Maranowski, and A. C. Gossard, Science **289**, 2323 (2000).

[3] M. A. Topinka, B. J. LeRoy, R. M. Westervelt, S. E. J. Shaw, R. Fleischmann, E. J. Heller, K. D. Maranowski, and A. C. Gossard, Nature (London) **410**, 183 (2001).

[4] B. Ludolph, M. H. Devoret, D. Esteve, C. Urbina, and J. M. van Ruitenbeek, Phys. Rev. Lett. **82**, 1530 (1999).

[5] C. Untiedt, G. Rubio Bollinger, S. Vieira, and N. Agraït, Phys. Rev. B **62**, 9962 (2000).

[6]Y. Zhang, P. Wahl, and K. Kern, Nano Lett. **11**, 3838 (2011).
[7]L. Limot, J. Kröger, R. Berndt, A. Garcia-Lekue, and W. A. Hofer, Phys. Rev. Lett. **94**, 126102 (2005).
[8]J. A. Stroscio and R. J. Celotta, Science **306**, 242 (2004).
[9]A. Sperl, J. Kröger, and R. Berndt, Phys. Rev. B **81**, 035406 (2010).
[10]S. D. Kevan and R. H. Gaylord, Phys. Rev. B **36**, 5809 (1987).
[11]M. F. Crommie, C. P. Lutz, and D. M. Eigler, Nature (London) **363**, 524 (1993).
[12]Y. Hasegawa and Ph. Avouris, Phys. Rev. Lett. **71**, 1071 (1993).
[13]L. Bürgi, O. Jeandupeux, H. Brune, and K. Kern, Phys. Rev. Lett. **82**, 4516 (1999).
[14]M. F. Crommie, C. P. Lutz, and D. M. Eigler, Science **262**, 218 (1993).
[15]See Supplemental Material at http://link.aps.org/supplemental/10.1103/PhysRevB.87.205417 for supplemental tables and figures.
[16]J. M. Krans, J. M. van Ruitenbeek, V. V. Fisun, I. K. Yanson, and L. J. de Jongh, Nature (London) **375**, 767 (1995).
[17]L. Limot, E. Pehlke, J. Kröger, and R. Berndt, Phys. Rev. Lett. **94**, 036805 (2005).
[18]F. E. Olsson, M. Persson, A. G. Borisov, J.-P. Gauyacq, J. Lagoute, and S. Fölsch, Phys. Rev. Lett. **93**, 206803 (2004).
[19]L. Bürgi, L. Petersen, H. Brune, and K. Kern, Surf. Sci. **447**, L157 (2000).
[20]L. Limot, T. Maroutian, P. Johansson, and R. Berndt, Phys. Rev. Lett. **91**, 196801 (2003).
[21]J. Kliewer, R. Berndt, and S. Crampin, Phys. Rev. Lett. **85**, 4936 (2000).
[22]N. Néel, J. Kröger, R. Berndt, and E. Pehlke, Phys. Rev. B **78**, 233402 (2008).
[23]A. Yazdani, D. M. Eigler, and N. D. Lang, Science **272**, 1921 (1996).
[24]A. Nitzan and M. A. Ratner, Science **300**, 1384 (2003).
[25]F. Sols, M. Macucci, U. Ravaioli, and K. Hess, Appl. Phys. Lett. **54**, 350 (1989).
[26]S. Datta, Superlattices Microstruct. **6**, 83 (1989).
[27]F. Capasso and S. Datta, Phys. Today (2) **43**, 74 (1990).
[28]T. J. Thornton, Rep. Prog. Phys. **58**, 311 (1995).
[29]Tapan Gupta, *Copper Interconnect Technology* (Springer, New York, 2009).